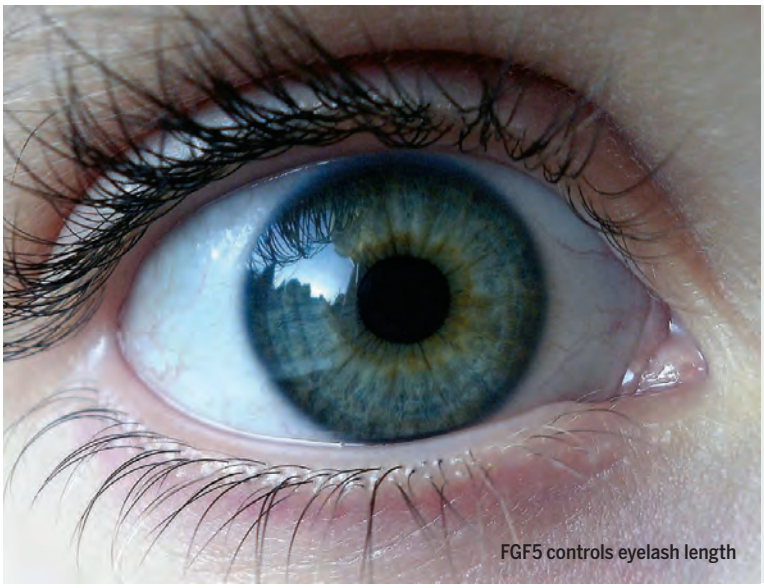

FGF5 controls eyelash length

DEVELOPMENT

The long and short of hair growth

The length of your eyelashes probably differs from the length of the hair on your head—and unlike your hair, your eyelashes can never reach your shoulders. What controls how long hair can get? To find out, Higgins *et al*. studied people with a rare disorder called familial trichomegaly, who have very long eyelashes and longer hair on the arms. They found that these people had a mutation in the gene that encodes fibroblast growth factor 5 (FGF5). When human hair follicles produce FGF5, they stop growing hair. Targeting FGF5 could potentially control the growth and rest phases of hair follicles, preventing unwanted hair from sprouting or growing longer lashes and locks. — LC

Proc. Natl. Acad. Sci. U.S.A. 10.1073/pnas.1402862111 (2014).

EDUCATION

Promoting evidence-based teaching

Empirical studies of science educational methods illuminate the best practices for getting students to learn. But why don't more science educators use such evidence-based teaching methods in their classrooms? They might not have access to the studies, DeChenne *et al.* report. The authors examined the role of practitioner-focused, discipline-based education research (DBER) journals in promoting and encouraging postsecondary teachers to adopt laboratory exercises supported by education research. Results showed a missed opportunity: DBER journals publish only a limited number of evidence-based instructional practices. — MM

J. Coll. Sci. Teach. **43**, 89 (2014).

ELECTRON TRANSFER

Electron tunneling or flickering resonance?

When electrons move from one site to another in biological molecules and the transfer drops off exponentially with distance, physicists usually assume they're seeing the electrons quantum-tunneling through energy barriers. A theoretical study by Zhang *et al.* provides a different interpretation. Molecules with the right combination of sites, with energy levels that align fleetingly during structural fluctuations, can produce the same decay signature. These "flickering resonances" temporarily create a band-like state for the electron, and as more sites are involved (corresponding to longer distances), the probability of creating the resonance drops exponentially. This mechanism operates over scale lengths of up to about 15 angstroms and could explain the short-distance electron transfer between bases in DNA. — PDS

Proc. Natl. Acad. Sci. U.S.A. 10.1073 pnas.1316519111 (2014).

MARINE BIOLOGY

Ship strikes threaten blue whale numbers

Whale-ship collisions may be behind low blue whale population counts despite international protections. Irvine *et al*. used satellites to track 171 blue whales off California over 15 years. The whales, part of the eastern North Pacific population, returned each summer to krill-rich upwelling zones off Santa Barbara and San Francisco—areas also crossed by major shipping lanes. At least three blue whales were killed by ship strike during 2 weeks in 2007. But a similar problem in Canada's Bay of Fundy offers hope: Eleven years ago, its maritime industry moved a shipping lane and reduced speed limits, reducing the likelihood of vessels striking right whales by 80%. — VM

A blue whale killed by a ship strike

PLOS ONE 10.1371/journal.pone.0102959(2014).

MICROBIAL PATHOGENS

How to make a not-so-painful ulcer

Buruli ulcer disease causes extensive skin lesions and can be deadly, but the lesions themselves don't hurt, which can stop patients from seeking the appropriate care. The pathogen *Mycobacterium ulcerans* causes Buruli ulcers and also alleviates the pain. Although many scientists studying this disease thought the pathogen caused nerve damage that blocked the pain, Marion *et al.* now show that the mycobacteria produce the mycolactone toxin, which causes analgesia by blocking the function of pain-responsive nerves. The findings could potentially help researchers develop a whole new class of painkillers. — SMH

Cell **157**, 1565 (2014).

GEOPHYSICS

Ample explanation for seismic variation

Geophysicists use seismic waves to make images of Earth's interior, but how they interpret those pictures depends on the properties of the minerals that make up the mantle. Wu and Wentzcovitch show that when the electron configuration of the iron in one of the most abundant minerals in the mantle, ferropericlase, changes at depths of 1000 km and greater, so does the way seismic waves propagate. The authors discuss several seismic features of the mantle previously thought to reflect different arrangements of minerals, such as compressional wave speed variations at depths of around 1750 km. Such features could be due not to mineralogy but to this electronic spin effect. — BG

Proc. Nat. Acad. Sci. U.S.A. 10.1073 pnas.1322427111 (2014).

PHOTOS: (TOP TO BOTTOM) KAREN ROE/FLICKR; FLIP NICKLIN/MINDEN PICTURES

Biological charge transfer via flickering resonance

Yuqi Zhang[a], Chaoren Liu[a], Alexander Balaeff[a,1], Spiros S. Skourtis[b,2], and David N. Beratan[a,c,d,2]

Departments of [a]Chemistry, [c]Biochemistry, and [d]Physics, Duke University, Durham, NC 27708; and [b]Department of Physics, University of Cyprus, Nicosia 1678, Cyprus

Edited by Jay R. Winkler, California Institute of Technology, Pasadena, CA, and accepted by the Editorial Board May 9, 2014 (received for review September 1, 2013)

Biological electron-transfer (ET) reactions are typically described in the framework of coherent two-state electron tunneling or multistep hopping. However, these ET reactions may involve multiple redox cofactors in van der Waals contact with each other and with vibronic broadenings on the same scale as the energy gaps among the species. In this regime, fluctuations of the molecular structures and of the medium can produce transient energy level matching among multiple electronic states. This transient degeneracy, or flickering electronic resonance among states, is found to support coherent (ballistic) charge transfer. Importantly, ET rates arising from a flickering resonance (FR) mechanism will decay exponentially with distance because the probability of energy matching multiple states is multiplicative. The distance dependence of FR transport thus mimics the exponential decay that is usually associated with electron tunneling, although FR transport involves real carrier population on the bridge and is not a tunneling phenomenon. Likely candidates for FR transport are macromolecules with ET groups in van der Waals contact: DNA, bacterial nanowires, multiheme proteins, strongly coupled porphyrin arrays, and proteins with closely packed redox-active residues. The theory developed here is used to analyze DNA charge-transfer kinetics, and we find that charge-transfer distances up to three to four bases may be accounted for with this mechanism. Thus, the observed rapid (exponential) distance dependence of DNA ET rates over distances of $\lesssim$15 Å does not necessarily prove a tunneling mechanism.

vibronic coupling | resonant tunneling pathways | superexchange | coherence | gated transport

Chemical structure and, importantly, structural fluctuations determine the mechanism and kinetics of charge transfer. Redox energy fluctuations are of particular significance when transport barrier heights and the energy fluctuations are of similar magnitude. Indeed, the sensitivity of biological electron-transfer (ET) rates to conformational fluctuations and consequent (transient) delocalization is the topic of intense interest (1–3). Resonant enhancement of biological ET rates is consistent with a growing body of physical and structural data found in DNA ET through stacked nucleobases (4), extended delocalized structures of bacterial photosynthesis (including the special pair, bridging chlorophyll and pheophytin) (5), the polaronic states of oxidized porphyrin arrays up to seven porphyrin diameters in spatial extent (6), micrometer-scale bacterial nanowires (7, 8), multiheme oxidoreductases (9, 10), amino acid side chains in ribonucleotide reductase (11), engineered protein-based hopping-chains (12), and centimeter-scale charge-transport chains in filamentous bacteria (13). Here, we describe a transient or flickering resonance (FR) mechanism for ET. The FR mechanism arises when thermal fluctuations produce geometries that enable charge delocalization across the entire structure by bringing the donor (**D**), bridge (**B**), and acceptor (**A**) levels into energetic degeneracy. An electron or hole that is spatially localized at a starting **D** may move ballistically (i.e., with near constant velocity) through these fleeting structures to **A**. Because the probability of bringing multiple sites into energetic degeneracy is multiplicative and decays approximately exponentially with the number of sites (i.e., with distance), this transport mechanism could be mistaken for electron tunneling because of its distance dependence.

ET Kinetics

The analysis in this paper concerns multisite charge transfer. Conventional biological ET theory is based on two-state dynamics (2, 14–16), with **D** and **A** brought into electronic resonance by medium reorganization. At resonance, the electron propagates from **D** to **A** either by tunneling (through space or via a bridge, **B**) i.e., nonadiabatic ET, or by strong electronic mixing among **D**, **B**, and **A** (adiabatic ET). Here, we explore a limit where the intrinsic energy fluctuations and/or medium reorganization create multistate electronic degeneracy and we demonstrate that charge transport in the degenerate state results in exponential distance dependence of the ET rate in both adiabatic and nonadiabatic regimes.

Two-State ET. To set the stage for the generalized flickering resonance (FR) mechanism, we explain this framework in the context of two-state **D**-to-**A** ET where the **D** and **A** energies are modulated by independent harmonic fluctuations. In this case, the FR picture is the standard picture of ET, where transfer takes place in thermally populated **D**–**A** resonances, within a redox energy matching window equal to the **D**-to-**A** coupling. To frame this discussion, we adopt the simplest kinetic model for two-state ET

$$\mathbf{D}^-\mathbf{A} \underset{k_{off}}{\overset{k_{on}}{\rightleftharpoons}} \mathbf{R}_2^{\ddagger}(\mathbf{D}^-\mathbf{A}) \xrightarrow{1/\tau_{trans}} \mathbf{R}_2^{\ddagger}(\mathbf{D}\mathbf{A}^-) \xrightarrow{1/\tau_{trap}} \mathbf{D}\mathbf{A}^-. \quad [1]$$

The overall **D**-to-**A** electron or hole transfer rate is denoted k_{ET}. $\mathbf{D}^-$ is the initially prepared state with an electron or hole on **D** in a state that is not resonant (R) with **A**. $\mathbf{R}_2^{\ddagger}(\mathbf{D}^-\mathbf{A})$ and $\mathbf{R}_2^{\ddagger}(\mathbf{D}\mathbf{A}^-)$ denote the subensemble of structures with **D** and **A** in two-state resonance and the electron on **D** or **A**, respectively. $\mathbf{DA}^-$ denotes the ET product with the electron or hole on the relaxed acceptor. k_{on} is the rate to reach two-state resonance $\mathbf{R}_2^{\ddagger}(\mathbf{D}^-\mathbf{A})$,

Significance

Electron transport through DNA plays a central role in nucleic acid damage and repair, and it is usually modeled using a carrier tunneling mechanism (at short distances) and a hopping mechanism (at longer distances). We find that fluctuations into transient geometries that bring multiple bases into electronic degeneracy may support band-like transport during the resonance lifetimes over a distance of $\lesssim$15 Å, obviating the need to invoke electron tunneling at short distances. This line of research may help to reveal mechanisms of charge transport in multiheme proteins, bacterial nanowires, and synthetic nanowires, and may also assist in framing the mechanisms of coherent multipigment excitonic transport in light-harvesting proteins.

Author contributions: Y.Z., C.L., A.B., S.S.S., and D.N.B. designed research, performed research, contributed new reagents/analytic tools, analyzed data, and wrote the paper.

The authors declare no conflict of interest.

This article is a PNAS Direct Submission. J.R.W. is a guest editor invited by the Editorial Board.

[1]Present address: NanoScience Technology Center, University of Central Florida, Orlando, FL 32826.

[2]To whom correspondence may be addressed. E-mail: david.beratan@duke.edu or skourtis@ucy.ac.cy.

This article contains supporting information online at www.pnas.org/lookup/suppl/doi:10.1073/pnas.1316519111/-/DCSupplemental.

$1/\tau_{trans}$ is the inverse time for electron transfer at resonance, and $1/\tau_{trap}$ is the trapping rate (considered irreversible in the context of transition state theory). The overall ET rate in this kinetic scheme is

$$k_{ET} = (1/\tau_*)\exp[-\Delta G_{act}/K_BT]. \quad [2]$$

For nonadiabatic ET, $\Delta G_{act} = \Delta G^{NA}_{act} = (\Delta G^{(0)}_{f,i} + \lambda)^2/4\lambda$ and $1/\tau_* = 2\pi V^2/\hbar\sqrt{4\pi\lambda K_BT}$. For adiabatic ET, $\Delta G_{act} = \Delta G^{AD}_{act}$ and, if ET is limited by k_{on}, then $1/\tau_* = \omega$ is the reaction coordinate motion attempt frequency. If ET is limited by solvent relaxation and/or by trapping, $1/\tau_* = 1/\tau_{trap}$ (e.g., $\tau_{trap} \approx \tau_L$ is the longitudinal relaxation time). Approximate expressions can be derived for ΔG^{AD}_{act}. For example, when $\Delta G^{(0)}_{f,i} = 0$, $\Delta G^{AD}_{act} = (\lambda/4) - |V|$ (15). In our FR reformulation of two-state (**D**-to-**A**) ET,

$$k_{ET} = (1/\tau)P_{match}(2), \quad [3]$$

where $P_{match}(2)$ is the probability that the **D** and **A** energy levels differ by less than the **D**–**A** electronic coupling V. If we assume independent energy level fluctuations for **D** and **A** sites, as well as independent fluctuations of the coupling V, then $P_{match}(2) = \int_{-\infty}^{+\infty} dV P_V(V) \int_{-\infty}^{+\infty} dE_1 \rho_1(E_1) \int_{E_1-|V|}^{E_1+|V|} dE_2 \rho_2(E_2)$, where $\rho_1(E_2)$ and $\rho_2(E_2)$ are the probability distribution functions for the electronic redox energies of the ET active states of sites 1 and 2. This formulation extends Hopfield's description of ET rates in terms of Gaussian broadened electron removal and insertion spectral functions (16). In Eq. **3**, $1/\tau$ is generally different from $1/\tau_*$ because $P_{match}(2) \neq \exp[-\Delta G_{act}/K_BT]$. For example (*SI Text*, section S4), in the approximation of constant coupling ($P(V) = \delta(V - |V_0|)$), the exact two-state matching probability is

$$P_{match}(2) = \left(\theta/\sqrt{2\pi}\right)\exp\left(-\left(\Delta G^{(0)}_{i,f} + \lambda - V_*\right)^2/4\lambda K_BT\right), \quad [4]$$

where $\theta = 2|V_0|/\sqrt{2\lambda K_BT}$, $\lambda = \lambda_D + \lambda_A$ is the total reorganization energy, and $V_* \in (-|V_0|, +|V_0|)$. Eq. **4** is valid in both the adiabatic ($\theta \geq 1$) and nonadiabatic ($\theta \ll 1$) regimes. From Eq. **4**, we see that τ in Eq. **3** is related to τ_* in Eq. **2** by the exact relation $1/\tau_* = (\theta/\sqrt{2\pi}) \times 1/\tau$ in any regime. In the nonadiabatic regime we have $\theta \ll 1$ and $\tau \ll \tau_*$. Further, in the nonadiabatic regime, $P_{match}(2) \approx P^{NA}_{match}(2)$, where $P^{NA}_{match}(2) = (\theta/\sqrt{2\pi})\exp(-\Delta G^{NA}_{act}/K_BT)$ and $\Delta G^{NA}_{act} = (\Delta G^{(0)}_{i,f} + \lambda)^2/4\lambda$ (*SI Text*, section S4). Thus, we can write the nonadiabatic rate either as $k^{NA}_{ET} = (1/\tau_*)\exp(-\Delta G^{NA}_{act}/K_BT)$ with $1/\tau_* = 2\pi V_0^2/\hbar\sqrt{4\pi\lambda K_BT}$ or $k^{NA}_{ET} = (1/\tau)P^{NA}_{match}(2)$, where, using $1/\tau_* = (\theta/\sqrt{2\pi}) \times 1/\tau$, we find $\tau = \tau_{Rabi}/\pi^2$ ($\tau_{Rabi} \equiv h/(2|V_0|)$ is the Rabi time). Moreover, $P^{NA}_{match}(2) = 2|V_{DA}| \times FC$, where FC is the well-known Franck–Condon factor: $FC = \langle\delta(E_{final} - E_{in})\rangle = (\sqrt{4\pi\lambda K_BT})^{-1}\exp(-\Delta G^{NA}_{act}/K_BT)$ (*SI Text*, section S4). In the adiabatic limit we have $\theta \approx 1$ and $\tau \leq \tau_*$. Importantly, when $\Delta G^{(0)}_{i,f} = 0$, $P_{match}(2) \approx (1/3)\exp(-\Delta G^{AD}_{act}/K_BT)$, where $\Delta G^{AD}_{act} = (\lambda/4) - |V_0|$ and $\tau = \tau_*/3$ (*SI Text*, section S4). As such, we have two equivalent strategies to formulate the two-state ET rate (Eqs. **2** and **3**). An advantage of using the matching probability (Eq. **3**) in formulating the ET rate is that it proves a computationally accessible means to estimate ET rates without first assuming a limiting coupling regime (i.e., adiabatic or nonadiabatic), and it enables generalization to multistate resonance.

A Generalized ET Rate for Multistate Resonance. For two-states, the FR rate is identical to two-state ET rates (adiabatic or nonadiabatic, depending on the magnitude of V_{DA}). For an N-state system, the FR mechanism defines a particular ET channel (other channels could well coexist). The FR kinetic model and the rate associated with FR are formulated in analogy to the above approach with the kinetic scheme

$$\mathbf{D}^-\mathbf{B}_{N-2}\mathbf{A} \underset{k_{off}}{\overset{k_{on}}{\rightleftharpoons}} \mathbf{R}^{\ddagger}_N(\mathbf{D}^-\mathbf{B}_{N-2}\mathbf{A}) \xrightarrow{1/\tau_{trans}} \mathbf{R}^{\ddagger}_N(\mathbf{DB}_{N-2}\mathbf{A}^-) \xrightarrow{1/\tau_{trap}} \mathbf{DB}_{N-2}\mathbf{A}^-. \quad [5]$$

$R^{\ddagger}{}_N(\mathbf{D}^-\mathbf{B}_{N-2}\mathbf{A})$ and $R^{\ddagger}{}_N(\mathbf{DB}_{N-2}\mathbf{A}^-)$ denote the subensemble of structures with all N units (including **D** and **A**) in degeneracy and the electron on **D** or **A**, respectively. $\mathbf{DB}_{N-2}\mathbf{A}^-$ is the product with the trapped electron on **A**, and P_{match} is the probability of matching all N states.

The FR channel ET rate is

$$k^{FR}_{ET} = (1/\tau_*)\exp(-\Delta G_{act(N)}/K_BT) \quad \text{or} \quad k^{FR}_{ET} = (1/\tau)P_{match}(N). \quad [6]$$

$\Delta G_{act(N)}$ is the activation free energy to reach N-state **D**–**B**–**A** resonance and τ_* is the rate-limiting time scale associated with the kinetics (k^{-1}_{on}, τ_{trans}, or τ_{trap} for the N-state system). In **[5]**, τ_{trans} is interpreted as the **D**-to-**A** transport time for N-state **D**–**B**–**A** resonance with a finite lifetime. The minimum value of τ_{trans} is obtained in the infinite FR lifetime limit, which gives $\tau^{min}_{trans} \approx \tau^{bal}_{trans} \approx R_{\mathbf{DA}}\,\hbar/(2r_{nn}V_{nn})$ [using a mean carrier velocity $\langle v\rangle = (1/\hbar[\partial E(k)/\partial k])|_{E_{Fermi}} = 2r_{nn}|V_{nn}|/\hbar$, where r_{nn} is the nearest-neighbor distance (17)]. For a nearest-neighbor coupling of 0.1 eV and a 3.4-Å separation among neighbors, the carrier velocity is ~1 Å/fs which places τ^{min}_{trans} in **[5]** in the range of tens of femtoseconds for a few redox sites. The τ_{trans} step in **[5]** generates transient carrier population on the bridge independent of the process that ultimately limits the overall rate of the FR channel (**[5]**).

As in the two-state limit, we could develop a multistate description where $k^{FR}_{ET} = (1/\tau_*)\exp(-\Delta G_{act(N)}/K_BT)$. However, the $P_{match}(N)$ formulation is particularly convenient in terms of computation and interpretation because of its explicit treatment of the influence of nearest-neighbor coupling on the energy-matching window (Fig. S1). For an N-state system with uncorrelated redox energy fluctuations, the probability of simultaneously matching all levels, summed over all matching energies, is

$$P_{match}(N) = \int_{-\infty}^{+\infty} dV P_V(V) \int_{-\infty}^{+\infty} dE_1 \rho_1(E_1) \int_{\varepsilon_1-|V|}^{\varepsilon_1+|V|} dE_2 \rho_2(E_2) \ldots \int_{max\{\varepsilon_1, \varepsilon_2, \ldots \varepsilon_{N-1}\}-|V|}^{min\{\varepsilon_1, \varepsilon_2, \ldots \varepsilon_{N-1}\}+|V|} dE_N \rho_N(E_N). \quad [7]$$

The upper limit of integration for the Nth site takes the minimum value of all site energies for sites 1 to $N-1$ plus $|V|$, and the lower limit of the Nth site integral takes the maximum value of all site energies for sites 1 to $N-1$ minus $|V|$. In this study, the matching probabilities are calculated using numerical integration for fewer than six sites and are computed using Monte Carlo methods for larger systems (18). We can derive exact expressions for $P_{match}(N)$ or $\Delta G_{act(N)}$ that are valid for arbitrary intersite couplings and can also derive corresponding relations between τ_* and τ (*SI Text*, section S4). In general, $P_{match}(N) = f \times \exp(-\Delta G_{act(N)}(\{E_i\}, \{V_{rms(i)}\}, \{\lambda_i\})/K_BT)$, where, approximately, $f \propto \theta_i^{N-1}$, with $\theta_i = V_{rms(i)}/\sigma_{E(i)}$, where $\sigma_{E(i)} = \sqrt{2\lambda_i K_BT}$ is the rms fluctuation of the ith site redox energy (and λ_i is the corresponding redox site reorganization energy), and $V^{rms}_{(i)}$ is the ith nearest-neighbor coupling. θ_i is

interpreted as a local (nearest-neighbor) adiababticity parameter, $\theta_i = \tau_{FC(i)}/\tau_{Rabi(i)}$. The FC time $\tau_{FC(i)} = h/\sqrt{2\lambda_i K_B T}$ is the time associated with the loss of the nearest-neighbor resonance arising from energy fluctuations of the ith site. $\tau_{Rabi(i)} = h/2V_{(i)}^{rms}$ is the Rabi time associated with resonance between sites i and $i+1$. Therefore, $f \propto \theta_i^{N-1}$ is a generalized N-state resonance adiabaticity parameter (*SI Text*, section S4). Even if nearest-neighbor resonances are quasiadiabatic with θ_i slightly less than unity, the N-state resonance becomes nonadiabatic as N grows because $f \propto \theta_i^{N-1}$. Thus, the effective lifetime of the N-state resonance decreases with increasing N. In Eq. **6**, $(\tau/\tau_*) \propto f$ and, in a generalized nonadiabatic limit defined by $f \ll 1$, we have $\tau_* \gg \tau$. If the overall rate is limited by carrier transmission through the N-state resonance, τ_* in Eq. **6** is interpreted as τ_{trans}, where $\tau_{trans} \approx \tau_{trans}^{bal}/f$ and τ_{trans}^{bal} is in the range of tens of femtoseconds for a few redox sites. That is, the nonadiabatic electron transmission time through the FR bridge is the band transport time increased by a nonadiabatic factor associated with degeneracy breaking.

Below, we describe a simple analytical approximation to Eq. **7** for a bridge with uncorrelated fluctuations, equal average site energies, and site energy fluctuations larger than coupling energy fluctuations (nonadiabatic limit). Importantly, (*i*) $P_{match}(N)$ decays exponentially with N; (*ii*) the distance dependence of $P_{match}(N)$ coincides with the slope of the hole transfer rates and yields in the experiments of Lewis et al. (19) and Giese et al. (20), for reasonable values of the hole transfer rate parameters; and (*iii*) fits to experimental ET rates and yields require $\tau \approx 1-15$ fs. To identify the rate-limiting step associated with the kinetic scheme of **[5]**, it is necessary to consider τ_*, which is longer than τ. Different possibilities for the rate-limiting steps are discussed below.

The Multisite Matching Probability

As a starting point, we assume statistically independent fluctuations for the multiple sites in the ET system. Standard deviations (σ_E, SD) for DNA base energies estimated from quantum mechanical (QM) analysis of molecular dynamics (MD) sampled structures indicate $\sigma_E \approx 0.2$ eV without solvent (21–23); inclusion of solvent interactions increases these values to ~0.3–0.5 eV (24, 25). Fig. S1 shows multisite energy-matching probabilities for a four-site linear system with Gaussian fluctuations of equal mean energies ($\sigma_E = 0.16$ eV), and with nearest-neighbor couplings fixed at $|V_{nn}| = 10^{-1}$, 10^{-2}, or 10^{-3} eV. Fig. S1 indicates that the four-site energy matching probability drops several orders of magnitude for each order of magnitude decrease in $|V_{nn}|$, because smaller values of $|V_{nn}|$ require closer site energy matching to establish FR.

The probability of matching N fluctuating site energies will decrease in a multiplicative fashion, with one multiplier per site. The energy-matching probability thus drops exponentially with distance. The data in Fig. S2 show the exponential decay of energy level-matching probabilities for a homogeneous chain (solid line) and an inhomogeneous chain (dashed line). For the homogeneous chain, all sites have the same mean energy values and $\sigma_E = 0.6$ eV; each nearest-neighbor coupling has zero mean and $V_{rms} = 0.1$ eV (the SD of the coupling magnitudes). For the inhomogeneous chains, **D** and **A** have the same mean energy values, whereas the bridging site energies are offset by 1 eV. The distance between neighboring sites is assumed to be 3.4 Å. In the case where all of the sites have the same mean energy (Fig. S2, solid line), the exponential decay constant for the matching probability as a function of distance is ~0.6 Å^{-1}. In the inhomogeneous case (Fig. S2, dashed line), the exponential decay constant is ~0.7 Å^{-1}. Thus, the average decay exponent increases as the energy offsets grow among the sites. The matching probability is several-fold smaller for the inhomogeneous chains compared with the homogeneous chains, although the decay of the matching probabilities with distance is not very different (because the bridging spectral functions are energy matched to one another in both cases).

The simple exponential distance dependence of the energy matching probabilities found in Fig. S2 is readily understood using an approximate model. Consider a chain with site energies that are described as independent Gaussian random variables with zero means and identical nonzero SDs, σ_E. The joint probability density function for the N-site redox energies is $\rho(E_1) \times \rho(E_2) \times \ldots \times \rho(E_N)$, where $\rho(E) = \left(1/\sqrt{2\pi\sigma_E^2}\right) e^{-E^2/2\sigma_E^2}$. An upper bound to the energy-matching probability is approximately $P_{match}(N) \approx (2\int_0^{V_{rms}} dE\rho(E))^N$. Because $V_{rms}/\sigma_E \approx 1/6$ in the example above, we can expand the exponential functions in terms of $(E/\sigma_E)^2$. Retaining the zeroth-order term, we find $P_{match}(N) \approx (\sqrt{2/\pi}(V_{rms}/\sigma_E))^N$ or

$$P_{match}(N) \approx e^{-\Phi R}, \quad \Phi = (1/\Delta R)\ln\left[\sqrt{\pi/2}(\sigma_E/V_{rms})\right] \qquad [8]$$

for a distance ΔR between adjacent sites [corrections to this result are found by retaining higher-order terms in $(E/\sigma_E)^2$]. For the inhomogeneous case of Fig. S2, a similar argument leads to $P_{match}(N) \approx e^{-E_B^2/2\sigma_E^2} e^{-\Phi R}$, where E_B is the mean energy gap between the **D**/**A** states and the N sites of the bridge. Using the values of Fig. S2 (typical for DNA), i.e., $V_{rms} = 0.1$ eV and $\sigma_E = 0.6$ eV, we find that $\Phi \approx 0.6$ Å^{-1} for a 3.4-Å spacing between bases. This is an excellent approximation to the numerical values found in Fig. S2. For the inhomogeneous system in Fig. S2, the decay of the **D**-to-**A** rate for the superexchange mechanism would be proportional to the square of the **B**-mediated **D**–**A** tunneling matrix element $V_{DA}^2 \propto e^{-\beta R_{dA}}$, where $\beta \approx$ (2/3.4 Å) ln $[(\Delta E_B/V_{rms})]$ in the perturbative limit (1, 2, 26, 27). Substituting $V_{rms} = 0.1$ eV and $\Delta E_B = 1$ eV gives $\beta \approx 1.4$ Å^{-1}. As such, for the parameters used in the illustration, the FR mechanism has much softer distance dependence than the superexchange rate. This simple analytical argument is strictly valid for $V_{rms}/\sigma_E < 1$ (the generalized nonadiabatic limit described above), and it can be used to assess the relative distance dependence of superexchange compared with FR as a function of V_{rms}, σ_E, and ΔE_B. An approximately exponential distance decay of the matching probability is also observed in molecular dynamics simulations and is discussed below. This simple analysis thus captures the source of the matching probability distance dependence. The crucial point from the above analysis is that FR transport requires all N – 2 bridging level energies to match each other, and the **D** and **A** energies; this matching probability drops exponentially with distance.

Correlated vs. Uncorrelated Site Energy Fluctuations

The illustrative FR computations above assume that site energy fluctuations for each site are uncorrelated Gaussians with $\sigma_{E_i} \approx \sqrt{2\lambda_i K_B T}$ (15, 16). Numerical simulations of Elstner demonstrate that the site energy fluctuations of neighboring bases in DNA are strongly correlated (25, 28). Mixed quantum/classical simulations indicate approximately Gaussian distributed site energy distributions (25, 29, 30) and nearest-neighbor electronic coupling distributions (25, 28, 31–34). However, the site energy fluctuation correlations break the simple connections between σ_E, λ, and $K_B T$, and produce values of $\lambda \approx 1.2$ eV. Below, we compute the level-matching probabilities P_{match} (N) using molecular dynamics simulations that include correlated energy level fluctuations.

The FR Model for DNA Charge Transport Kinetics

Limitations of Current Models. A large body of experimental data indicates two regimes of DNA charge transfer: a regime with strong (exponential) dependence of the rate/yield on distances up to ~3–7 bp and a much weaker dependence for longer distances (35). Theoretical models have focused on describing short-distance

transport with a tunneling model and longer-distance transport with a multistep or multirange hopping approach (36, 37). This framework has challenges associated with understanding transient **B** population in an apparent tunneling regime and with describing the transition between strong and weak distance-dependent regimes (*SI Text*, section S1 and refs. 4, 19, 21, 22, 30, and 38–41).

FR Descriptions of Charge Shift and Charge Separation in DNA. The highest occupied molecular orbital (HOMO) energies of DNA bases are often used to estimate site energies in simple transport models (42, 43). The site energies of purines are higher than those of pyrimidines, so hole transfer is dominated by the purines. It is found that thermal fluctuations of the DNA bases produce distributions of base (gas phase) HOMO energies that are found to be approximately Gaussian distributed (25). Quantum mechanics/molecular mechanics (QM/MM) simulations that include solvent interactions further broaden the site energy distributions, producing increased probabilities of level matching even for sites with different mean energies (i.e., with different redox potentials). DNA sampling and energy computation protocols based on a model AT sequence, including correlated site energy fluctuations, are described in *SI Text*, section S2 (21, 22, 25, 28, 29, 44, 45), and these data are required for the FR kinetic analysis discussed below.

Charge Shift in the FR Framework. We used the MD-derived parameters in the FR model to describe hole transfer and trapping in DNA systems studied by Giese et al. (20). As indicated in Fig. S3, a hole is injected onto a G site via photoexcitation of a 4′-acylated nucleotide. From there, the hole can either be lost to solvent in a chemical reaction that converts the G to an 8-oxoG, or it can propagate across an AT bridge to a lower-energy GGG state and exit to solvent from that unit (Fig. S3). The location of the 8-oxoG is then revealed through strand cleavage with piperidine, and the chemical yield ratio P_{GGG}/P_G for the cleavage products at the injection site G or the destination site GGG is measured using gel electrophoresis (20). Thus, the P_{GGG}/P_G ratio provides a measure of the G→GGG charge-transfer rate compared with the G→8-oxoG oxidation rate. The distance dependence of the P_{GGG}/P_G ratio is studied by varying the number of (AT) base pairs from 1 to 16 between the G and GGG traps.

Three spectral functions were introduced for the donor G, the bridge adenines (A), and the acceptor GGG (Fig. S4). The energy gap between the peaks of the spectral functions was set to $\Delta G + \lambda$ where ΔG is the free energy of charge shift between the sites and λ is the reorganization energy. ΔG is the charge shift reaction free energy for donor G to A or GGG. The free energy change for $G^{+\bullet}A$ to $GA^{+\bullet}$ ET is +0.35 eV (19) and from $G^{+\bullet}(GGG)$ to $G(GGG)^{+\bullet}$ is −0.7 eV (46). Typical λ values for DNA ET range from 0.4 eV (nearest-neighbor) to 1.2 eV (four **B** units between **D** and **A**) (45, 47). Smaller free energy differences between G and GGG states were reported as well (*ca.* 0.08 eV) (48). Decreased trapping free energies can also be accommodated in the FR model.

The FR probabilities for Giese's structures are calculated using sampling from both MD and distribution functions using the energetics shown in Fig. S4 and a normally distributed energy matching window randomly selected from a Gaussian distribution with zero mean and SD of 0.1 eV, as described above with G–A couplings of 0.043 eV and A–A couplings of 0.08 eV (44). The FR charge-transfer rate is modeled with Eq. **6**, where τ is an adjustable parameter used to fit the absolute values of the yields.

To compare our simulations with the experimental chemical yield ratios (P_{GGG}/P_G), we use the kinetic model (49) suggested by Jortner and coworkers. In this model, the water-trapping rate for the holes on GGG is assumed to be much larger than the back charge transfer (CT) rate, i.e., all of the holes that arrive at GGG are trapped. Therefore, the yield ratio is determined by the ratio of the charge transport rate and the trapping rate of the single G, $P_{GGG}/P_G \approx k_{CT}/k_r$. We set the trapping rate k_r to be $\sim 2.0 \times 10^9\ s^{-1}$, consistent with the earlier estimate of Jortner et al. (49). Giese and Spichty estimated the water-trapping rate to be as low as $\sim 6.0 \times 10^4\ s^{-1}$ (50), based on a tunneling rate through two **B** sites of $2.5 \times 10^6\ s^{-1}$ (51).

The computed and experimental chemical yield ratios are shown in Table 1. In the short-distance regime, the calculated chemical yield ratios have an exponential decay parameter of $\beta \approx 0.5\ Å^{-1}$, in good agreement with experimental data. As the chain length grows beyond 3–4 bp, the hole transfer presumably becomes dominated by incoherent (hopping) transport, and the FR mechanism is no longer relevant.

Application of the FR Model to DNA Hairpins. We also used the coupling and site energy distribution functions described above in the FR model to explore charge transfer in stilbene-capped DNA hairpins studied by Lewis et al. (19, 41) (Fig. S5). In their experiments, hole transfer occurs between the photoexcited stilbene electron donor Sd and electron acceptor Sa separated by one to six AT bridging base pairs (19). In contrast to the Giese system, hole transfer between the stilbenes produces the charge-separated state $Sa^{-\bullet}/Sd^{+\bullet}$. The electron hole attraction in that state creates a **D**–**A** charge separation energy ramp (Fig. S6; cf. ref. 21), in addition to the redox potential difference between the stilbenes and adenines.

The mean energies of the spectral functions at each site are computed from the analysis of Grozema et al.: $\langle E_i \rangle = E_{ion}(A) - E_{el.aff}(Sa) - E_{exc}(Sa) - E_{elst}(A^{+\bullet}Sa^{-\bullet}) - \Delta E_{solv}$. Here, $E_{ion}(A)$ is the gas-phase ionization potential of adenine in the DNA stack, $E_{el.aff}(Sa)$ is the vacuum electron affinity of Sa, $E_{exc}(Sa)$ is the optical excitation energy, and $E_{elst}(A^{+\bullet}Sa^{-\bullet})$ is the D/A Coulomb interaction in the charge-separated state (21). The SDs of these energy distribution functions are set to 0.6 eV, similar to the values from Elstner's QM/MM analysis of DNA (25). If the excited state has exciplex character with partial delocalization onto the DNA, the site energies should be decreased.

Using the protocol described to treat site energy correlations, we calculated the matching probability for DNA hairpins (with one to three intervening ATs). The energy ramp produces large energy gaps between sites for systems with more than three AT bridging units, making the probability negligible to form a degenerate geometry at these larger distances. We therefore focus our study of the FR mechanism on $Sa(A)_nSd$ ($n = 1, 2, 3$) DNA hairpins. In the energy matching probability analysis for the $Sa(A)_nSd$ DNA, the nearest-neighbor coupling is taken to be normally distributed around zero with a SD of 0.1 eV (44). The FR charge-transfer rate is modeled with Eq. **6**, where τ is an adjustable parameter used to fit the absolute values of the rates. The computed β-value is consistent with the measured kinetic data (Table 2).

Rate-Limiting Time Scales. The distance dependence of the FR matching probability $P_{match}(N)$ is consistent with the measured distance dependence of the charge shift yields (Table 1) and charge separation rates (Table 2) at short distances. We have not

Table 1. Computed P_{match}, experimental yield ratios, and fitted τk_r values (with k_r the water-trapping rate) for data of Giese et al. (20) (see Scheme S1)

Bridge units	P_{match}	P_{GGG}/P_G	$\tau k_r \times 10^5$
1	4.8×10^{-3}	250	1.9
2	8.5×10^{-4}	30	2.8
3	2.1×10^{-4}	4	5.2
4	6.0×10^{-5}	3.5	1.7

Table 2. Computed P_{match}, experimental hole arrival rates of Lewis et al. (19), and fitted τ values

Bridge units	P_{match}	$k_{arrival}^{Expr}$, ns^{-1}	τ, fs
1	7.6×10^{-3}	580	13.1
2	2.1×10^{-4}	27	7.8
3	5.3×10^{-5}	3.4	15.6
4	1.3×10^{-5}	1	13.0

assumed a particular ET regime (adiabatic or nonadiabatic), and it is remarkable that the slope of the distance dependence of DNA rates and yields is predicted successfully by the MD-derived $P_{match}(N)$. Our only fitting parameter is τ in Eq. **6**. Recall that the time scale of the rate-limiting step (τ_* in Eq. **6**) in the generalized kinetic scheme of **[5]**, is related to τ by $(\tau_*/\tau) \propto \prod_{i=1}^{N-1} \theta_i^{-1}$ where $\theta_i \approx V_{rms}/\sigma_E$, regardless of the reaction adiabaticity. Assuming $\theta_i \approx 1/3$ to $1/6$ for the DNA systems studied here, τ_* is in the tens of femtoseconds to picoseconds range for the photoinduced charge separation experiments, and τ_* is in the hundreds of nanoseconds to tens of microseconds for the charge shift (yield) experiments. Which step(s) in **[5]** determine τ_*? We do not expect τ_{trap} to depend strongly on distance, so it is not likely to be equal to τ_*. τ_{trans} could be the origin of τ_* in the charge separation experiments because the fitted τ (Table 2) is as fast as tens of femtoseconds. However, we also expect k_{on} to be distance dependent (**[5]**), because $\Delta G_{act(N)}$ is distance dependent and so is the attempt frequency to form the N-state FR. Therefore, k_{on}^{-1} could determine τ_* in both experiments, and it could be the rate-limiting step for FR (we expect k_{on} to differ for charge shift and charge separation reactions). For ultrafast ET, it is possible that the time scale determining the ET rate prefactor will differ for different observation time windows, as ET active species can be depleted and replenished on multiple time scales.

In summary, the FR mechanism is compatible with the slopes of the distance dependences of the rates and yields in the charge separation and charge shift experiments at shorter distances. However, our analysis cannot resolve whether the FR channel is rate limited by the time scale of D–B–A transport in the N-state resonance conformation or by the activation rate to the N-state resonance conformation. Regardless of the rate-limiting kinetic step, the signatures of the FR mechanism are the exponential rate decay with distance and a transient carrier population on the bridge.

Conclusions

The FR probability drops approximately exponentially as a function of distance, so FR transport has a signature that can be mistaken for tunneling. This theoretical framework provides a scheme to quantify ideas of how stacking dynamics may influence the coherence of charge transfer. The FR mechanism is consistent with observed ET rates in hole transfer experiments of Giese et al. and Lewis et al. FR explains exponential distance decay of rates in the presence of transient **D** and **A** carrier populations that do not sum to unity as they must in the superexchange regime.

The redox energy-matching probability depends critically on nearest-neighbor couplings and energy gaps, as well as on their fluctuations. Level matching can be substantial, even when the **D**, **B**, and **A** sites are nonresonant on average. Fluctuations are expected to depend on temperature, structure, flexibility, and coupling pathway interferences. As such, one should be able to manipulate the energy-matching propensity. In particular, the FR model predicts approximately exponential distance dependence for the ET rate with decay exponent $\Phi \propto \ln(\sigma_E/V_{rms}) \propto \ln(\sqrt{2\lambda KT}/V_{rms})$. This characteristic behavior provides a specific testable signature for the FR mechanism.

Disrupting energy level matching during electron transmission, combined with relaxation, can produce multirange hopping or mixed hopping and superexchange (30, 40). Future studies need to track the carrier dynamics that follows the disruption of resonance, to set more precise bounds on the admixture of coherent, incoherent, and mixed transport. The lessons of the present study are that FR (*i*) obviates the need to invoke tunneling in short distance DNA ET, (*ii*) rationalizes the observation of electron arrival at the **A** population without the concomitant reduction of the **D** population in a DNA hairpin that also displays steep distance-dependent ET rates, and (*iii*) suggests new approaches to controlling ET by varying site energy and coupling distributions. Building further on the isomorphism between energy and ET kinetics (16), it seems likely that the framework described here may be of use for analyzing coherences among excitonic states of artificial and natural light-harvesting complexes (52–59).

ACKNOWLEDGMENTS. We thank Mark Ratner, Fred Lewis, Bernd Giese, and Ron Naaman for their thoughtful feedback on the ideas described here. Support from Office of Naval Research–Multidisciplinary University Research Initiative N00014-11-1-0729 (to A.B., Y.Z., and D.N.B.) for studies of DNA charge transport mechanisms and from National Science Foundation CHE-1057953 (to C.L. and D.N.B.) in support of nucleic acids coherence phenomena are gratefully acknowledged.

1. Beratan DN, et al. (2009) Steering electrons on moving pathways. *Acc Chem Res* 42(10):1669–1678.
2. Skourtis SS, Waldeck DH, Beratan DN (2010) Fluctuations in biological and bioinspired electron-transfer reactions. *Annu Rev Phys Chem* 61:461–485.
3. Skourtis SS (2013) Review: Probing protein electron transfer mechanisms from the molecular to the cellular length scales. *Biopolymers* 100(1):82–92.
4. Muren NB, Olmon ED, Barton JK (2012) Solution, surface, and single molecule platforms for the study of DNA-mediated charge transport. *Phys Chem Chem Phys* 14(40): 13754–13771.
5. Blankenship RE (2002) *Molecular Mechanisms of Photosynthesis* (Blackwell Science, Oxford).
6. Susumu K, Frail PR, Angiolillo PJ, Therien MJ (2006) Conjugated chromophore arrays with unusually large hole polaron delocalization lengths. *J Am Chem Soc* 128(26): 8380–8381.
7. El-Naggar MY, et al. (2010) Electrical transport along bacterial nanowires from Shewanella oneidensis MR-1. *Proc Natl Acad Sci USA* 107(42):18127–18131.
8. Malvankar NS, Tuominen MT, Lovley DR (2012) Comment on "on Electrical Conductivity of Microbial Nanowires and Biofilms" by S. M. Strycharz-Glaven, R. M. Snider, A. Guiseppi-Elie and L. M. Tender, *Energy Environ Sci*, 2011, 4, 4366. *Energy Environ Sci* 5(3):6247–6249.
9. Mowat CG, Chapman SK (2005) Multi-heme cytochromes—new structures, new chemistry. *Dalton Trans* (21):3381–3389.
10. Breuer M, Rosso KM, Blumberger J (2014) Electron flow in multiheme bacterial cytochromes is a balancing act between heme electronic interaction and redox potentials. *Proc Natl Acad Sci USA* 111(2):611–616.
11. Stubbe J, Nocera DG, Yee CS, Chang MCY (2003) Radical initiation in the class I ribonucleotide reductase: Long-range proton-coupled electron transfer? *Chem Rev* 103(6):2167–2201.
12. Shih C, et al. (2008) Tryptophan-accelerated electron flow through proteins. *Science* 320(5884):1760–1762.
13. Pfeffer C, et al. (2012) Filamentous bacteria transport electrons over centimetre distances. *Nature* 491(7423):218–221.
14. Gray HB, Winkler JR (2003) Electron tunneling through proteins. *Q Rev Biophys* 36(3): 341–372.
15. Marcus RA, Sutin N (1985) Electron transfers in chemistry and biology. *Biochim Biophys Acta* 811(3):265–322.
16. Hopfield JJ (1974) Electron transfer between biological molecules by thermally activated tunneling. *Proc Natl Acad Sci USA* 71(9):3640–3644.
17. Ashcroft N, Mermin D (1976) *Solid State Physics* (W. B. Saunders, Philadelphia).
18. Wolfram Research, Inc (2012) Mathematica (Champaign, IL), Version 9.0.
19. Lewis FD, et al. (2006) Crossover from superexchange to hopping as the mechanism for photoinduced charge transfer in DNA hairpin conjugates. *J Am Chem Soc* 128(3): 791–800.
20. Giese B, Amaudrut J, Köhler A-K, Spormann M, Wessely S (2001) Direct observation of hole transfer through DNA by hopping between adenine bases and by tunnelling. *Nature* 412(6844):318–320.
21. Grozema FC, et al. (2008) Effect of structural dynamics on charge transfer in DNA hairpins. *J Am Chem Soc* 130(15):5157–5166.
22. Hatcher E, Balaeff A, Keinan S, Venkatramani R, Beratan DN (2008) PNA versus DNA: Effects of structural fluctuations on electronic structure and hole-transport mechanisms. *J Am Chem Soc* 130(35):11752–11761.
23. Venkatramani R, Keinan S, Balaeff A, Beratan DN (2011) Nucleic acid charge transfer: Black, white and gray. *Coord Chem Rev* 255(7-8):635–648.
24. Voityuk AA, Siriwong K, Rösch N (2004) Environmental fluctuations facilitate electron-hole transfer from guanine to adenine in DNA pi stacks. *Angew Chem Int Ed Engl* 43(5):624–627.

25. Kubar T, Kleinekathöfer U, Elstner M (2009) Solvent fluctuations drive the hole transfer in DNA: A mixed quantum-classical study. *J Phys Chem B* 113(39):13107–13117.
26. Beratan D, Skourtis S (1998) Electron transfer mechanisms. *Curr Opin Chem Biol* 2(2): 235–243.
27. Skourtis SS, Beratan DN (1999) Theories of structure-function relationships for bridge-mediated electron transfer reactions. *Adv Chem Phys* 106:377–452.
28. Kubar T, Elstner M (2008) What governs the charge transfer in DNA? The role of DNA conformation and environment. *J Phys Chem B* 112(29):8788–8798.
29. Grozema FC, et al. (2009) Effect of GC base pairs on charge transfer through DNA hairpins: The importance of electrostatic interactions. *J Am Chem Soc* 131(40):14204–14205.
30. Renaud N, Berlin YA, Lewis FD, Ratner MA (2013) Between superexchange and hopping: An intermediate charge-transfer mechanism in poly(A)-poly(T) DNA hairpins. *J Am Chem Soc* 135(10):3953–3963.
31. Kubař T, Elstner M (2013) Efficient algorithms for the simulation of non-adiabatic electron transfer in complex molecular systems: Application to DNA. *Phys Chem Chem Phys* 15(16):5794–5813.
32. Kubar T, Elstner M (2009) Solvent reorganization energy of hole transfer in DNA. *J Phys Chem B* 113(16):5653–5656.
33. Kubar T, Elstner M (2010) Coarse-grained time-dependent density functional simulation of charge transfer in complex systems: Application to hole transfer in DNA. *J Phys Chem B* 114(34):11221–11240.
34. Voityuk AA (2007) Fluctuation of the electronic coupling in DNA: Multistate versus two-state model. *Chem Phys Lett* 439(1-3):162–165.
35. Schuster GB, ed (2004) Long-range charge transfer in DNA I and II. *Top Curr Chem* (Springer, Berlin), Vol 236–237.
36. Berlin YA, Kurnikov IV, Beratan D, Ratner MA, Burin AL (2004) DNA electron transfer processes: Some theoretical notions. Long-range charge transfer in DNA II. *Top Curr Chem* 237:1–36.
37. Jortner J, Bixon M, Voityuk AA, Rosch N (2002) Superexchange mediated charge hopping in DNA. *J Phys Chem A* 106(33):7599–7606.
38. Skourtis S, Nitzan A (2003) Effects of initial state preparation on the distance dependence of electron transfer through molecular bridges and wires. *J Chem Phys* 119(12):6271–6276.
39. Bixon M, Jortner J (2005) Incoherent charge hopping and conduction in DNA and long molecular chains. *Chem Phys* 319(1-3):273–282.
40. Renger T, Marcus RA (2003) Variable-range hopping electron transfer through disordered bridge states: Application to DNA. *J Phys Chem A* 107(41):8404–8419.
41. Lewis FD, et al. (2008) Getting to guanine: Mechanism and dynamics of charge separation and charge recombination in DNA revisited. *Photochem Photobiol Sci* 7(5):534–539.
42. Paul A, et al. (2009) Role of nucleobase energetics and nucleobase interactions in single-stranded peptide nucleic acid charge transfer. *J Am Chem Soc* 131(18):6498–6507.
43. Venkatramani R, et al. (2011) Evidence for a near-resonant charge transfer mechanism for double-stranded peptide nucleic acid. *J Am Chem Soc* 133(1):62–72.
44. Voityuk AA (2008) Electronic couplings and on-site energies for hole transfer in DNA: Systematic quantum mechanical/molecular dynamic study. *J Chem Phys* 128(11):115101.
45. LeBard DN, Lilichenko M, Matyushov DV, Berlin YA, Ratner MA (2003) Solvent reorganization energy of charge transfer in DNA hairpins. *J Phys Chem B* 107(51): 14509–14520.
46. Sugiyama H, Saito I (1996) Theoretical studies of GG-specific photocleavage of DNA via electron transfer: Significant lowering of ionization potential and 5′-localization of HOMO of stacked GG bases in B-form DNA. *J Am Chem Soc* 118(30):7063–7068.
47. Olofsson J, Larsson S (2001) Electron hole transport in DNA. *J Phys Chem B* 105(42): 10398–10406.
48. Lewis FD, Liu J, Zuo X, Hayes RT, Wasielewski MR (2003) Dynamics and energetics of single-step hole transport in DNA hairpins. *J Am Chem Soc* 125(16):4850–4861.
49. Bixon M, et al. (1999) Long-range charge hopping in DNA. *Proc Natl Acad Sci USA* 96(21):11713–11716.
50. Giese B, Spichty M (2000) Long distance charge transport through DNA: Quantification and extension of the hopping model. *ChemPhysChem* 1(4):195–198.
51. Lewis FD, et al. (2000) Direct measurement of hole transport dynamics in DNA. *Nature* 406(6791):51–53.
52. Scholes GD (2003) Long-range resonance energy transfer in molecular systems. *Annu Rev Phys Chem* 54:57–87.
53. Fidler AF, Singh VP, Long PD, Dahlberg PD, Engel GS (2013) Timescales of coherent dynamics in the light harvesting complex 2 (LH2) of *Rhodobacter sphaeroides*. *J Phys Chem Lett* 4(9):1404–1409.
54. Fransted KA, Caram JR, Hayes D, Engel GS (2012) Two-dimensional electronic spectroscopy of bacteriochlorophyll a in solution: Elucidating the coherence dynamics of the Fenna-Matthews-Olson complex using its chromophore as a control. *J Chem Phys* 137(12):125101.
55. Fidler AF, Caram JR, Hayes D, Engel GS (2012) Towards a coherent picture of excitonic coherence in the Fenna–Matthews–Olson complex. *J Phys B-At Mol Opt* 45(15):154013.
56. Fleming GR, Scholes GD (2004) Physical chemistry: Quantum mechanics for plants. *Nature* 431(7006):256–257.
57. Wong CY, et al. (2012) Electronic coherence lineshapes reveal hidden excitonic correlations in photosynthetic light harvesting. *Nat Chem* 4(5):396–404.
58. Schlau-Cohen GS, De Re E, Cogdell RJ, Fleming GR (2012) Determination of excited-state energies and dynamics in the B band of the bacterial reaction center with 2D electronic spectroscopy. *J Phys Chem Lett* 3(17):2487–2492.
59. Zaks J, Amarnath K, Kramer DM, Niyogi KK, Fleming GR (2012) A kinetic model of rapidly reversible nonphotochemical quenching. *Proc Natl Acad Sci USA* 109(39): 15757–15762.